Project 039 Naphthalene Removal Assessment

Massachusetts Institute of Technology

Project Lead Investigator

Steven R. H. Barrett
Professor of Aeronautics and Astronautics
Department of Aeronautics and Astronautics
Massachusetts Institute of Technology
77 Massachusetts Avenue, Bldg. 33-316
Cambridge, MA 02139
(617)-452-2550
sbarrett@mit.edu

University Participants

Massachusetts Institute of Technology

- PI(s): Professor Steven R. H. Barrett, Dr. Raymond Speth (Co-PI)
- FAA Award Number: 13-C-AJFE-MIT
- Period of Performance: July 8, 2016 to February 28, 2021
- Task(s):
    1. Preliminary screening of the naphthalene removal refining processes
    2. Calculation of process requirements and fuel composition effects for selected refining processes
    3. Estimate capital and operating costs of naphthalene removal
    4. Develop a kinetic model of polycyclic aromatic hydrocarbon (PAH) formation with fuel-composition effects
    5. Compare kinetic model results to laser flash-photolysis photoionization mass spectrometry (LFP/PIMS) experimental data
    6. Evaluate the relationship between PAH formation and aircraft particulate matter (PM) emissions
    7. Calculate air quality and climate impacts of naphthalene removal
    8. Conduct integrated cost–benefit analysis of impacts of naphthalene removal in the United States

Investigation Team

- Professor Steven Barrett (Massachusetts Institute of Technology [MIT]) served as PI for the A39 project as head of the Laboratory for Aviation and the Environment. Professor Barrett both coordinates internal research efforts and maintains communication among investigators in the various MIT research teams described below.
- Dr. Raymond Speth (MIT) served as co-PI for the A39 project. Dr. Speth directly advised students performing research in the Laboratory for Aviation and the Environment, with a focus on assessment of naphthalene removal refinery options; climate and air quality modeling; and fuel alteration life-cycle analysis. Dr. Speth also coordinated communication with FAA counterparts.
- Professor William Green (MIT) served as a co-investigator for the A39 project, as head of the Green Research Group. Professor Green advised students on work in the Green Research Group focusing on computer-aided chemical kinetic modeling of PAH formation.
- Mr. Randall Field (MIT) is the Executive Director of the MIT Energy Initiative and was a co-investigator of the A39 project. Drawing upon his experiences as a business consulting director at Aspen Technology Inc., Mr. Field provided mentorship to student researchers in the selection and assessment of naphthalene removal refining options and process engineering in general.
- Mr. Drew Weibel (MIT) was a graduate student researcher in the Laboratory for Aviation and the Environment. Mr. Weibel was responsible for conducting selection and assessment of naphthalene removal refining options; calculation of refinery process requirements and fuel composition effects from selected processes; estimation of capital and operating costs of naphthalene removal processes; air quality and climate modeling; and integrated cost–benefit analysis.
- Mr. Lukas Brink (MIT) was a graduate student researcher in the Laboratory for Aviation and the Environment. Mr. Brink was responsible for the development of a combustor model quantifying the effect of naphthalene removal on soot emissions, and the use of this model to assess air quality and climate impacts of naphthalene removal.

- Dr. Mica Smith (MIT) was a postdoctoral associate in the Green Research Group. Ms. Smith was responsible for the experimental measurements being used for the validation of the chemical kinetic mechanisms.
- Dr. Agnes Jocher (MIT) was a postdoctoral associate in the Green Research Group. Ms. Jocher was responsible for evaluating microphysical models that link the presence of PAH molecules to the formation of soot particles and for providing modeling expertise in combining these models with the kinetic models being developed.

Project Overview

The composition of aviation fuels affects the formation of pollutants that contribute to climate change and to reduced air quality that leads to adverse health impacts, including an increased risk of premature mortality. The objective of this project was to assess the societal costs and benefits of removing naphthalenes from jet fuel produced in the United States. Removal of naphthalene by extractive distillation has been found to be less expensive than hydrotreatment. Hydrotreatment has the additional effect of removing sulfur from the fuel, while fuel processed by extractive distillation has larger reductions in nvPM emissions. The largest environmental benefits come from reductions in air quality damages due to sulfur emissions, although the removal of sulfur also results in a net warming effect on the climate. The climate benefits due to reductions in nvPM emissions are mainly associated with reductions in contrail radiative forcing (RF). However, this benefit is more than offset by the increased CO_2 emissions required for the naphthalene removal processes. These results suggest that naphthalene removal on a nationwide basis is unlikely to be cost beneficial with either extractive distillation or hydrotreatment. However, naphthalene removal could be beneficial under certain circumstances, for example, if applied to fuels used at individual airports with particular air quality concerns, or if used at times and locations where the formation of warming contrails is most likely.

References

Brem, B. T., Durdina, L., Siegerist, F., Beyerle, P., Bruderer, K., Rindlisbacher, T., Rocci-Denis, S., Andac, M. G., Zelina, J., Penanhoat, O., & Wang, J. (2015). Effects of fuel aromatic content on nonvolatile particulate emissions of an in-production aircraft gas turbine. Environmental Science and Technology *49*, 13149–13157.

Moore, R. H., Shook, M., Beyersdorf, A., Corr, C., Herndon, S., Knighton, W. B., Miake-Lye, R., Thornhill, K. L., Winstead, E. L., Yu, Z., Ziemba, L. D. & Anderson, B. E. (2015). Influence of jet fuel composition on aircraft engine emissions: A synthesis of aerosol emissions data from the NASA APEX, AAFEX, and ACCESS missions. Energy Fuels *29*, 2591–2600.

Task 1 - Preliminary Screening of the Naphthalene Removal Refining Processes

Massachusetts Institute of Technology

Objective

Naphthalene is present at varying levels in the straight-run crude oil distillation cuts used to produce jet fuel and is currently not targeted for removal in the treatments used to meet industry standard fuel specifications. Consequently, reducing the naphthalenic content in jet fuel requires the introduction of an additional refinery treatment process. The objective of this task is to identify suitable refinery processes that could be used to remove or convert naphthalenes. Once identified, data for key refining process parameters will be collected to inform future cost estimation of applying the selected processes for jet fuel naphthalene removal.

Research Approach

Introduction

Refining processes, and chemical processes in general, are focused on subjecting chemical species to various environments to allow for conversion, combination, separation, etc. thus yielding useful products with increased value. When considering removal of a chemical component from a mixture, e.g., naphthalenic species from a kerosene feed, a process designer must consider the unique properties shared by the chemical component that allow for its conversion, combination, separation, etc. without affecting the underlying mixture.

Although naphthalenes are not currently targeted for removal to meet industry standards, several mature refining technologies, once tuned, could perform this reduction or removal with high efficiency. We selected suitable, readily accessible refining technologies for the removal of naphthalenes from the U.S. jet pool. Our focus is on technologies currently used in industry, to determine possible policies that could be implemented in the near term.

Methods

To select various refining processes for the large-scale removal of naphthalenes from the U.S jet fuel pool, we completed a literature review of current technologies, then performed a qualitative evaluation of those technologies in terms of their applicability to naphthalene removal, the scope of economic and process data available, and the level of naphthalene removal achievable. Particular attention was paid to preserving non-naphthalenic aromatic compounds, because reducing the amounts of these components would limit the ability to blend paraffinic alternative jet fuels while still meeting the minimum requirements for aromatics.

To evaluate each candidate process, we leveraged the existing literature to estimate the utility requirements (e.g., process fuel, electricity, or hydrogen) for each process, the effect on the composition of the resulting jet fuel, and the capital costs of new refinery equipment required. We included the effects of any potentially necessary pre-processing. We then compared processes side-by-side to demonstrate the trade-offs associated with naphthalene removal at the refinery.

In analyzing a range of different refining pathways, we will also be able to assess the tradeoffs associated with different levels of naphthalene removal. Those efforts, together with ongoing work regarding the relationship between jet fuel composition and PAH formation, will allow us to assess the level at which naphthalenes should be removed to optimize costs and benefits.

Results

This task concluded with the selection of extractive distillation and selective hydrotreating as candidate refinery processes for the large-scale removal of naphthalenes from the U.S. jet fuel pool.

Naphthalenes are unsaturated, double-ring aromatic species, that may contain alkylated or impurity groups. They are most readily removed via conversion to mono-aromatic or saturated species—via hydrogen addition or carbon removal—or separated on the basis of polarity. A desired refinery process would remove naphthalenic species with high efficiency without affecting the remaining aromatic content, would result in minimal changes to other fuel properties, and would produce limited emissions and economic impact; the removal of other impurities (e.g., sulfur or nitrogen) would also be preferable. A list of potential refining processes is shown in Figure 1 (Gary et al., 2007).

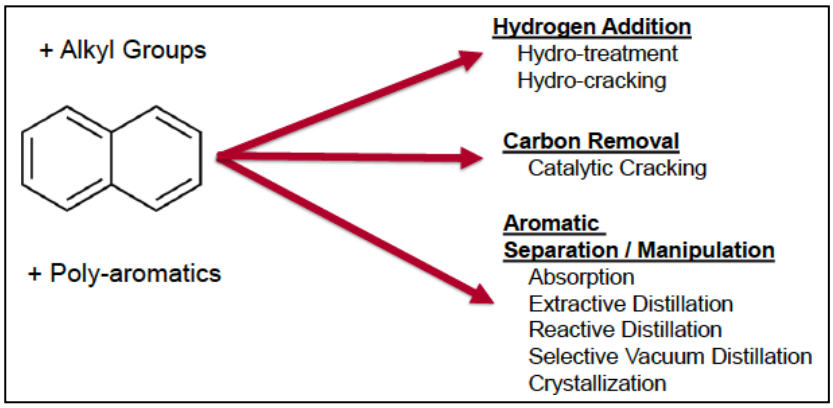

Figure 1. Categories of potential processes for naphthalene removal.

As noted, three families of processes are pertinent to the removal of naphthalenes: conversion by hydrogen addition (saturation), conversion by carbon removal (cracking), and aromatic separation. Hydrogen addition and aromatic separation are often used as finishing processes and can be performed under mild conditions. Carbon removal, in contrast, is often associated with molecular cracking, has the potential to radically convert the feed, is associated with the production of olefins, and often cannot break apart stable aromatic rings. As a result, only hydro-conversion and aromatic separation processes were considered.

Hydro-conversion processes are a family of refining units that react a petroleum feed with gaseous hydrogen at elevated temperatures and pressures to saturate—and in severe processes, crack—hydrocarbon molecules. Hydrotreating is a mild hydro-conversion finishing process used to remove impurities and saturate olefin and aromatic species. Selective hydro-treating for the conversion of naphthalenes is a viable process candidate because the second ring of naphthalenic species tends to be fully saturated before the saturation of mono-aromatic species. Because of the relative selectivity of fuel

components, we also expect desulfurization and di-nitrogenation to occur. As a result, with a robust catalyst selection and finely tuned process parameters, we expect that a selective hydrotreating process could reduce or remove naphthalenes by converting them to mono-aromatics, while resulting in little change to the overall aromatic content and other fuel characteristics, and having reasonable hydrogen requirements (Fahim et al., 2009).

Separation processes enable mixtures to be divided into their components according to defining species characteristics, such as weight, size, polarity, etc. Extractive distillation enables the separation of petroleum components based on polarity, by introducing a heavy, high-boiling point polar solvent to the feed. Highly polar components, including all aromatic and impurity-containing species, will bind to the solvent and be separated from other species according to weight. The solvent is then separated by simple distillation. Finally, mono-aromatic and naphthalene species can be roughly separated in a second distillation step, and the prior cut is returned to the feed. Extractive distillation, although less common for feed mixture separations, was identified as a second candidate for naphthalene removal from the U.S. jet fuel pool (Meyers, 2004).

After selection of extractive distillation and selective hydrotreating as candidate refining processes for the removal/reduction of naphthalene from the U.S. jet fuel pool, we collected further details on each process to define their offsite needs and fuel composition impacts. Table 1 shows the relevant process requirements and fuel effects.

Table 1. Process requirements and fuel impacts for hydrotreatment and extractive distillation.

Process Name	Hydrotreatment	Extractive Distillation
Description	Hydrogenation of naphthalenes to mono-aromatic and cyclo-paraffinic components	Separation of all aromatics via a polar solvent; separation of mono-aromatics from naphthalenes via distillation and subsequent blending back into the jet fuel product
Process Type	Conversion (H_2 addition)	Aromatic separation
Existing Uses	Desulfurization, impurity removal, aromatic hydrogenation	Separation of polar feed components, benzene, toluene, xylene (BTX) separation
Removal of Naphthalenes	Assumed 95% efficient	Assumed 95% efficient
Effect on Mono-Aromatics	Limited (<10%) hydrogenation	Fully separated; fraction returned to product can be controlled
Impurity Removal	S and N removal to < 50 ppm	Little removal of S and N impurities
Supporting Processes Required	Hydrogen production, sulfur gas removal, sulfur post-treatment, steam generation and cooling facilities	Naphthalene/mono-aromatic post distillation, steam generation and cooling facilities
Process Innovation Required	Minimal required; very similar to existing units	Efficient solvent with impurity (S and N) resiliency

Milestone

This task concluded with the selection of extractive distillation and selective hydrotreating as candidate refinery processes for the large-scale removal of naphthalenes from the U.S. jet fuel pool. The results were described in a presentation provided to the FAA on February 28, 2017.

Major Accomplishments

During this period, two refining processes—selective hydrotreating and extractive distillation—were chosen as suitable candidates for large-scale naphthalene removal from the U.S. jet fuel pool. A summary of this work is contained in the Deliverable 1 presentation provided to the FAA on February 28, 2017.

Publications

Weibel, D. (2018). Techno-economic assessment of jet fuel naphthalene removal to reduce non-volatile particulate matter emissions [S.M. thesis, Massachusetts Institute of Technology]. DSpace@MIT. https://hdl.handle.net/1721.1/124174

Outreach Efforts

ASCENT advisory board presentations/posters (April 2017, September 2017, and April 2018)

Student Involvement

Drew Weibel, a Master's student in the Laboratory for Aviation and the Environment, worked directly with Professor Steven Barrett and Dr. Raymond Speth to conduct the research objectives of Task 1.

References

Gary, J. H., Handwerk, G. E., & Kaiser, M. J. (2007). *Petroleum refining: Technology and economics* (5th ed.). CRC Press.

Fahim, M. A., Al-Sahhaf, T., & Elkilani, A. (2009). *Fundamentals of petroleum refining*. Elsevier Science.

Meyers, R. (2004). *Handbook of petroleum refining processes* (3rd ed.). McGraw-Hill.

Task 2 - Calculation of Process Requirements and Fuel Composition Effects for Selected Refining Processes

Massachusetts Institute of Technology

Objective

In Task 1, selective hydrotreating and extractive distillation were selected as candidate refinery processes for large-scale reduction or removal of naphthalene from the U.S. jet fuel pool. In addition, data were collected regarding the offsite (or supporting process) requirements and fuel composition effects of each process.

The objective of this task was to continue quantitative analysis of both processes to develop simplified estimation models of process requirements and fuel composition effects. The result of this task will be cost estimation for individual selective hydrotreating and extractive distillation refinery units, modeled as brown-field additions to existing refinery operations.

Research Approach

Methods

Based on the process parameters defined as part of Task 1, utility requirements and capital cost data were collected for distillate hydro treating, extractive distillation, and their supporting processes. The supporting processes of selective hydrotreating are steam methane reforming for hydrogen production, amine separation for hydrogen sulfide separation from off-gasses, and the Claus process for sulfur recovery. Because these supporting processes are often connected to several units at a refinery, costs were determined based on both the size of the modelled refinery and the capacity of the modelled hydro-treatment unit. The sole supporting process for extractive distillation is post-distillation.

To calculate the net present value (NPV) of an added refinery finishing process for the reduction or removal of naphthalene from jet fuel, the methods described by Gary et al. (2007) were adopted. Fixed capital investment was estimated from the desired process capacities and the collected cost data. Operating cost was calculated as a function of the fixed costs, and as a function of the utility requirements and estimated utility costs (depicted in Figure 2). Catalyst/solvent and process water utility costs were assumed to be constant (Gary et al. 2007, Peters et al., 2003). Historical and predicted natural gas and electricity prices, by U.S. census region, were taken from the U.S. Energy Information Administration. We used an autoregressive moving average model, calibrated to the predicted trend and historical price variations, to estimate natural gas and electricity prices stochastically. The NPV was then calculated with a discounted cash flow rate of return (DCFRoR) model over the lifetime of the process unit. A discount factor of 2.74%, according to the 20-year constant maturity rate, was used for the estimated cost to society.

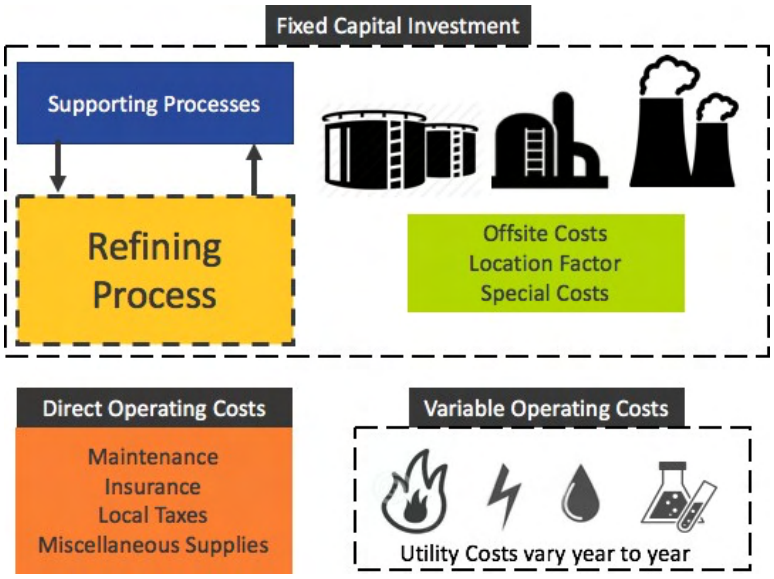

Figure 2. Schematic of factors affecting costs of refinery processes.

Results
The model successfully estimated the cost of the reduction or removal of naphthalene from U.S. jet fuel via operation of an additional finishing process (either selective hydrotreating or extractive distillation) at U.S. refineries. Preliminary cost data were presented in the Deliverable 3 presentation provided to the FAA on August 31, 2017.

Milestone
This work was completed in August 2017 and is summarized in the Deliverable 1-3 presentation provided to FAA on August 31, 2017.

Major Accomplishments
During this period, a simplified model was created for the purpose of cost estimation of individual selective hydrotreating and extractive distillation process units. This model included effects on fuel composition, utility requirements, and estimated costs over the lifetime of the unit. Results collected from the discounted cash flow model are presented as the NPV of the unit over its lifetime. A summary of this work is contained in Deliverable 1-3, provided to the FAA on August 31, 2017.

Publications
Weibel, D. (2018). Techno-economic assessment of jet fuel naphthalene removal to reduce non-volatile particulate matter emissions [S.M. thesis, Massachusetts Institute of Technology]. DSpace@MIT. https://hdl.handle.net/1721.1/124174

Outreach Efforts
- ASCENT advisory board presentations/posters (September 2017, April 2018, and October 2018)
- Presentation at the Coordinating Research Council Aviation Meeting (May 2018) titled “Naphthalene Removal Assessment: Cleaning up Jet Fuel for Reduced Environmental Impacts”
- Presentations at the Aviation Emissions Characterization (AEC) Roadmap Annual Meetings (May 2018 and May 2020)

Student Involvement
Drew Weibel, a Master’s student in the Laboratory for Aviation and the Environment, worked directly with Professor Steven Barrett and Dr. Ray Speth to conduct the research objectives of this task.

References

Gary, J. H., Handwerk, G. E., & Kaiser, M. J. (2007). *Petroleum refining: Technology and economics* (5th ed.). CRC Press.
Peters, M. S., Timmerhaus, K. D., & West, R. E. (2003). *Plant design and economics for chemical engineers*. (5th ed.). McGraw-Hill.

Task 3 - Estimate Capital and Operating Costs of Naphthalene Removal

Massachusetts Institute of Technology

Objective

The objective of this task was to evaluate refinery technologies that could be used to remove naphthalene, and to determine their feasibility, costs, and effects on fuel composition. This process included calculating the costs of constructing new refinery unit processes and determining additional utility and other operating costs associated with using the process units responsible for naphthalene removal.

Research Approach

Naphthalene is present at varying levels in the straight-run crude oil distillation cuts used to produce jet fuel. For cuts exceeding the 3% volume limit on naphthalenes (ASTM D1655 2016), this excess can be resolved solely through blending, because the average naphthalene content of commercial Jet A fuel is ~1.4% (DLA Energy 2013). Reducing or eliminating the naphthalene content of jet fuel would therefore require the introduction of additional refinery processing. After reviewing several candidate refining processes in the prior year of this project, we decided to further explore two processes in detail: selective hydrotreatment and extractive distillation. These processes are used in industry for the reduction or separation of aromatics, and they show promise in their ability to reduce and remove naphthalene from jet fuel. Selective hydrotreatment reacts hydrogen with the feedstock and leads to the removal of impurities and saturation of aromatic compounds. Extractive distillation allows for the full separation of aromatics from the feedstock via polar solvents. The aromatics stream can then be processed to separate mono-aromatics and naphthalenes, and the former stream is then returned to the jet fuel blending pool. These processes were chosen because of their low added complexity and energy, and their minimal effect on the resultant fuel properties. However, changes in fuel density, specific energy, fuel sulfur content, hydrogen content, and aromatic content will occur and were considered.

We have developed fundamental process models to estimate the effects of fuel constituents and completed a literature search to collect data on process energy requirements, capital costs, and operating costs for both hydrotreatment and extractive distillation. To evaluate each candidate process, we leveraged the existing literature to estimate the utility (e.g., process fuel, electricity, or hydrogen) requirements for each process, the effect on the composition of the resulting jet fuel, and the capital costs of new refinery equipment required, including the effects and costs of pre-processing and auxiliary process units that might be required. We then compared processes side by side to demonstrate the trade-offs associated with naphthalene removal at refinery.

We considered the hypothetical adoption of a policy whereby jet fuel naphthalene content in the U.S. is reduced by 95% via either hydrotreatment or extractive distillation, at each of the 116 operational U.S. refineries with capacities > 1,000 barrels per day (BPD). We calculated costs using a stochastic discounted cash flow model of each refinery. Refinery capital costs were calculated using standard cost curve estimation methods, which relate process unit costs to capacity. Cost curves were used for both the primary naphthalene-removing process units (e.g., extractive distillation column or hydrotreater) as well as auxiliary process units (e.g., steam-methane reformer, Claus sulfur recovery unit, pressure-swing hydrogen recovery units, and steam generators). Direct operating costs included maintenance, local taxes, insurance, and supplies, calculated as a percentage of capital costs. Variable operating costs, such as process water and chemicals, were calculated according to the process unit utility requirements. The stochastic refinery model was used to determine the NPV of each naphthalene removal process over its operating lifetime. The NPV could also be used to calculate the cost premium (i.e., cents per gallon) associated with the production of naphthalene-free fuel. Cost estimates were considered from two perspectives: that of the fuel market and that of society. The market perspective involved computation of cost premiums including all cash flows incurred by fuel producers, by estimating the expected increase in the market price for naphthalene-free jet fuel. The societal cost estimate was computed from a resource-based perspective, placing it on the same basis as the monetization of potential benefits from improved air quality and potential climate impacts. From that perspective, redistribution of resources, e.g., taxes or loan payments, was disregarded, and the discount rate was assumed to be equivalent to society's long-term cost of capital.

Milestone

The work completed for this task was documented in Deliverable 2-1, provided to the FAA on November 30, 2017.

Major Accomplishments

The resource-based (societal) cost premium and market cost premium estimate distributions for a policy in which all U.S.-produced jet fuel has its naphthalene content reduced by 95% (to 0.06 vol%) are shown in Figure 3, with cost data presented in 2016 USD. The mean societal cost premium was found to be 2.4 cents/liter (95% confidence interval (CI): 2.0–2.7) for hydrotreating and 1.7 cents/liter (95% CI: 1.5–1.0) for extractive distillation.

The mean market cost premium of hydrotreating was found to be 3.1 cents/liter (95% CI: 2.4–3.7), and that for extractive distillation was found to be 2.1 cents/liter (95% CI: 1.7–2.5). Given that the average U.S. Gulf Coast cost of jet fuel in 2016 was $0.33/liter, this represents a 9% and 6% increase in the cost of jet fuel for naphthalene removal via hydrotreatment and extractive distillation, respectively.

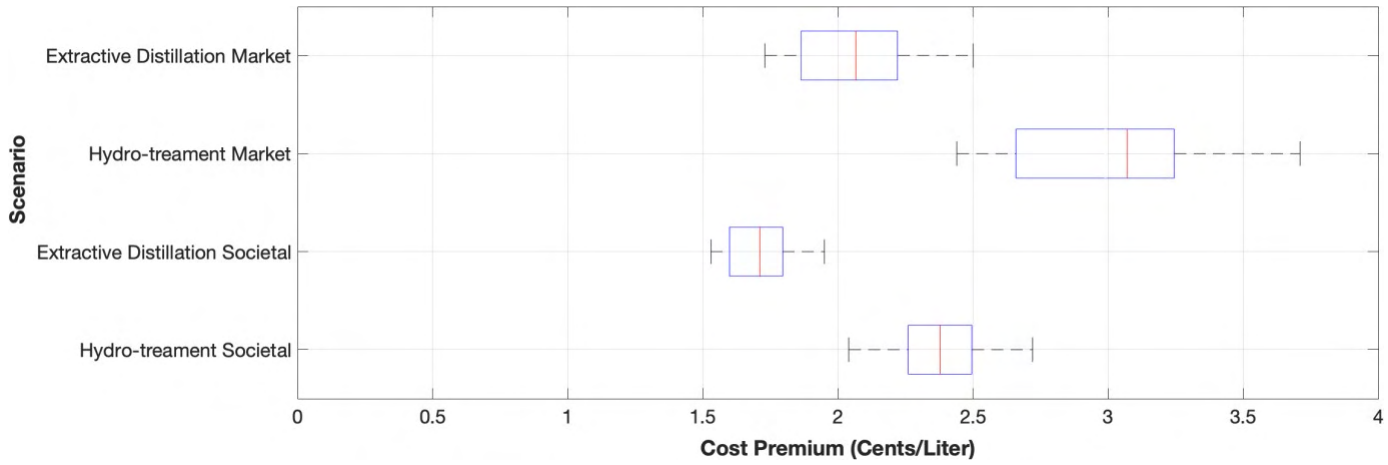

Figure 3. Box plot showing the societal and market cost premiums of hydrotreatment and extractive distillation. All values are in cents/liter. Red markers represent the distribution means, blue boxes represent the first and third quartiles, and whiskers represent the 95% CI.

Publications

Weibel, Drew (2018). Techno-economic assessment of jet fuel naphthalene removal to reduce non-volatile particulate matter emissions [S.M. thesis, Massachusetts Institute of Technology]. DSpace@MIT. https://hdl.handle.net/1721.1/124174

Outreach Efforts

- ASCENT advisory board presentations (September 2017, April 2018, and October 2018)
- Presentation at the CRC Aviation Meeting (May 2018) titled “Naphthalene Removal Assessment: Cleaning up Jet Fuel for Reduced Environmental Impacts”
- Presentation at the AEC Roadmap Annual Meeting (May 2018 and May 2020)
- Presentation at the CAEP/12-WG3/2 meeting (October 2019) titled “Economic and Environmental Assessment of Jet Fuel Naphthalene Removal”

Student Involvement

This task was conducted primarily by Drew Weibel, a Master’s student in the Laboratory for Aviation and the Environment, working directly with Professor Steven Barrett and Dr. Raymond Speth.

References

ASTM. (2016) *D1655: Standard Specification for Aviation Turbine Fuels*. ASTM International. https://doi.org/10.1520/D1655-16C

DLA Energy. (2013). Petroleum quality information system 2013 annual report (Report No. ADA619019). Defense Logistics Agency, Fort Belvoir, VA.

Task 4 · Develop a Kinetic Model of PAH Formation with Fuel-Composition Effects

Massachusetts Institute of Technology

Objective

The formation of black carbon (soot) from hydrocarbon fuels can be considered to occur in two stages. First, fuel components and combustion intermediates react to form polycyclic aromatic hydrocarbons (PAHs). Subsequently, large PAHs act as soot nuclei, which grow as they absorb both PAH and other species, coagulate through collisions with other soot particles, carbonize, and partially oxidize (Richter and Howard, 2000). The details of fuel composition mainly affect the first step of this process, the formation of PAHs. In this project, we used the Reaction Mechanism Generator (RMG) to develop a detailed chemical kinetic mechanism for jet fuel combustion including the formation of PAH (Gao et al., 2016).

The objective of this task was to update the RMG algorithm to accommodate aromatic species, and to include aromatic reactions up to three-ring species, for use as identifiers for soot precursors in later models. The updates to RMG also underwent preliminary validation according to experimental results from shock-tube pyrolysis and co-pyrolysis studies.

Research Approach

Introduction

RMG (http://rmg.mit.edu) is an automatic chemical reaction mechanism generator that constructs kinetic models composed of elementary chemical reaction steps using a general understanding of how molecules react. This tool provides a powerful method to computationally identify reaction mechanisms and ensure full coverage of pertinent species and reactions according to the current literature. RMG has been used to analyze various fuels including JP-10 and di-isopropyl ketone combustion and pyrolysis (Gao et al., 2015; Allen et al., 2014).

We will add updates to the RMG algorithm to accurately accommodate aromatic species, and to include aromatic reactions up to three-ring species, which will be used as identifiers for soot precursors in later models.

Method

Previously, RMG was unable to robustly represent aromatic structures. The algorithm depended primarily on representations using Kekulé structures, thus resulting in their incorrect treatment as aliphatic species. To correctly represent aromatic species, RMG was updated to generate Clar structure representations of PAHs. As result, aromatic species are more clearly differentiated from aliphatic species, and the number of representations has been reduced in many cases. An example of the decreased number of representations for a phenanthrene radical is shown in Figure 4.

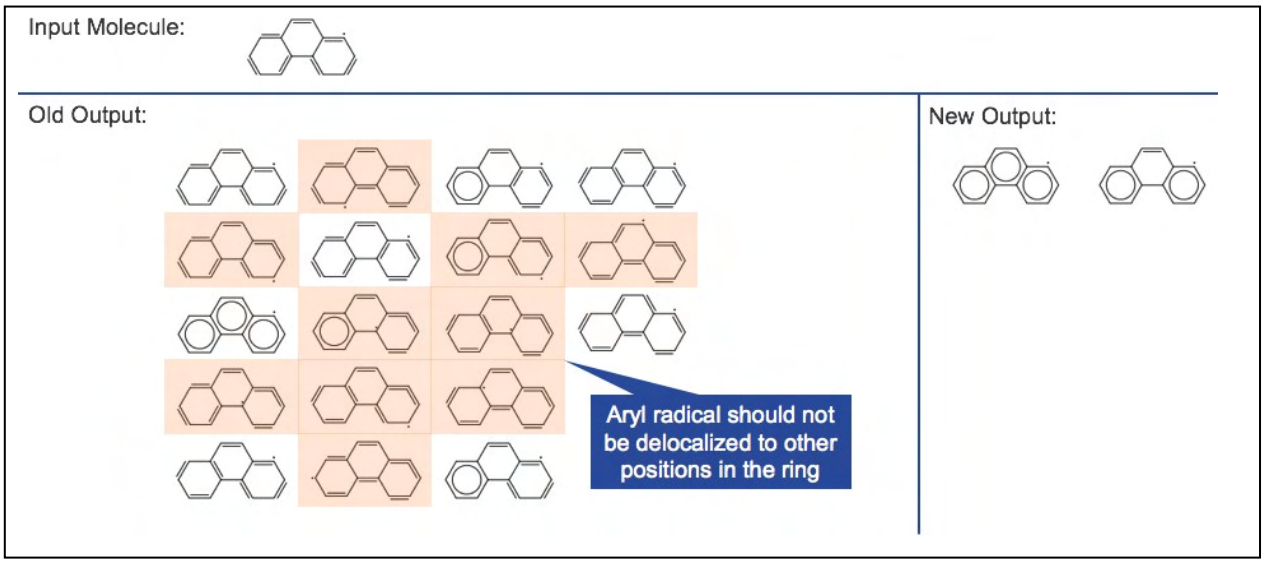

Figure 4. Kekulé and Clar structures for a phenanthrene radical.

Other changes were made to further improve the reaction rate predictions. An algorithmically challenging task of allowing aromatic bond types was completed after implementing a custom kekulization algorithm. This allows rate rules for aromatic species to be specified separately from those for aliphatic species. Moreover, ring perception was implemented for rate rules to allow for the separation of rates for linear versus cyclic species.

To validate the updates described previously, we tested the RMG model against experimental shock-tube pyrolysis data (Lifshitz et al., 2009). Additional co-pyrolysis models were also generated, although without experimental comparisons.

Results

The improvements described above successfully enabled RMG to handle aromatic species. Prior to the updates, program crashes were inevitable when modeling any aromatic system. To support the algorithm changes, new literature data for aromatic thermochemistry and kinetics were added to the database.

For preliminary validation, a model was generated for pyrolysis of 1-iodonaphthalene and acetylene for comparison to shock-tube data. The model predictions for the major products, acenaphthalene and naphthalene, matched the experimental data well, as shown in Figure 5. The RMG model predicted a higher yield of 1-ethynyl naphthalene than the literature model, although none was observed in the experiment. The RMG model also predicted smaller side products, such as vinylacetylene and 1,3-butadiene, which were not reported in the experiment, although the authors do note that small molecule products from acetylene reactions were assumed to be negligible.

Co-pyrolysis models for equimolar naphthalene or tetralin with acetylene were also generated to obtain an initial view regarding whether RMG could capture the differences in reactivity. For naphthalene and acetylene, RMG predicted the major products to be acenaphthalene and hydrogen, a finding that was initially surprising, because other PAHs such as anthracene or phenanthrene were also expected. However, these observations were corroborated by Parker et al. (2015), who have also observed that acenaphthalene is the main product, in contrast to the generally accepted hydrogen abstraction-C_2H_2 addition (HACA) mechanism for PAH growth. The model for tetralin and acetylene displayed markedly different behavior, as expected. Major products were hydrogen, naphthalene, methane, and ethene. No three-ring aromatics were formed, possibly because of the overall higher hydrogen/carbon ratio.

Overall, these modeling results are very promising and show that RMG is now much better at modeling aromatics.

Milestone(s)

This work was completed in June 2017 and is contained in the Deliverable 2 presentation provided on Jun 30, 2017.

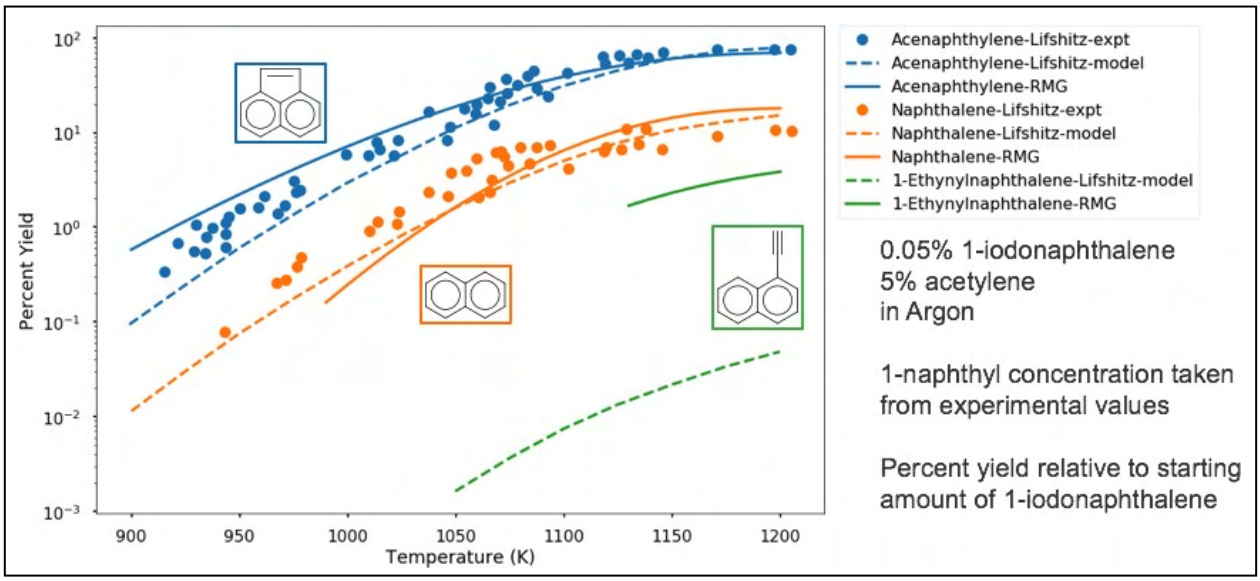

Figure 5. Comparison of yields for selected PAH species in shock tube experiments and kinetic models.

Major Accomplishments

During this period, the RMG algorithm was successfully updated to accommodate aromatic species, and kinetics data were added for aromatic species. These updates also underwent preliminary validation through comparison to experimental shock-tube pyrolysis data. A summary of this work is contained in the Deliverable 2 presentation provided to the FAA on June 30, 2017.

Publications

Liu, M., & Green, W. H. (2019). Capturing aromaticity in automatic mechanism generation software. Proceedings of the Combustion Institute, *37*(1), 575–581. https://doi.org/10.1016/j.proci.2018.06.006

Liu, M. (2020). Predictive modeling of polycyclic aromatic hydrocarbon formation during pyrolysis [Ph.D. thesis, Massachusetts Institute of Technology]. DSpace@MIT. https://hdl.handle.net/1721.1/129925

Outreach Efforts

- Presentation at the International Conference on Chemical Kinetics (May 2017) titled "Going Bigger: Capturing PAH Chemistry in RMG"
- Presentation at the Aviation Emissions Characterization (AEC) Roadmap Annual Meeting (June 2017)
- Presentation at the 37th International Symposium on Combustion (August 2018) titled "Capturing Aromaticity in Automatic Mechanism Generation Software"

Student Involvement

Mengjie (Max) Liu, a PhD student in the Green Research Group at MIT's Department of Chemical Engineering, completed the majority of the updates to the RMG, and validation and refinement of the RMG models.

References

Allen, J. W., Scheer, A. M., Gao, C. W., Merchant, S. S., Vasu, S. S., Welz, O., Savee, J. D., Osborn, D. L., Lee, C., Vranckx, S., Wang, Z., Qi, F., Fernandes, R. X., Green, W. H., Hadi, M. Z., & Taatjes, C. A. (2014). A coordinated investigation of the combustion chemistry of diisopropyl ketone, a prototype for biofuels produced by endophytic fungi. Combustion and Flame, *161*(3), 711–724. https://doi.org/10.1016/j.combustflame.2013.10.019

Gao C. W., Allen J. W., Green W. H., & West R. H. (2016). Reaction mechanism generator: Automatic construction of chemical kinetic mechanisms. Computer Physics Communications, *203*, 212–225. https://doi.org/10.1016/j.cpc.2016.02.013

Gao, C. W., Vandeputte, A. G., Yee, N. W., Green, W. H., Bonomi, R. E., Magoon, G. R., Wong, H.-W., Oluwole, O. O., Lewis, D. K., Vandewiele, N. M., & Van Geem, K. M. (2015). JP-10 combustion studied with shock tube experiments and modeled with automatic reaction mechanism generation. Combustion and Flame, *162*(8), 3115–3129. https://doi.org/10.1016/j.combustflame.2015.02.010

Lifshitz, A., Tamburu, C., & Dubnikova, F. J. (2009). Reactions of 1-naphthyl radicals with acetylene. Single-pulse shock tube experiments and quantum chemical calculations. Differences and similarities in the reaction with ethylene. Journal of Physical Chemistry A, *113*(39), 10446–10451. https://doi.org/10.1021/jp905448g

Parker, D. S. N., Kaiser, R. I., Bandyopadhyay, B., Kostko, O., Troy, T. P., & Ahmed, M. (2015). Unexpected chemistry from the reaction of naphthyl and acetylene at combustion-like temperatures. Angewandte Chemie, *54*(18), 5421–5424. https://doi.org/10.1002/ange.201411987

Richter, H., & Howard, J. B. (2000). Formation of polycyclic aromatic hydrocarbons and their growth to soot—a review of chemical reaction pathways. Progress in Energy and Combustion Science, *26*(4–6), 565–608. https://doi.org10.1016/S0360- 1285(00)00009-5

Task 5 - Compare Kinetic Model Results to LFP/PIMS Experimental Data

Massachusetts Institute of Technology

Objective

The growth of aromatic rings as part of PAH formation is controlled by radical reactions, particularly the HACA mechanism. The objective of this task was to produce experimental data that can be used to improve estimates of rate coefficients used in chemical kinetic models of PAH formation.

Research Approach

Laser flash-photolysis photoionization mass spectrometry (LFP/PIMS) is an experimental technique in which a photolysis laser pulse initiates controllable, quantifiable radicals in a temperature- and pressure-controlled reactor. The evolution of the chemical composition in the reactor is then monitored by ionization with VUV light and detection with a mass spectrometer. Experimental conditions were simulated with reactor modeling software, using rate coefficients estimated from the literature. Because these rate coefficients are often pressure dependent, quantum chemistry calculations were used to extrapolate from the low-pressure experimental values to the high pressures relevant to engine operations. Simulations using RMG-generated mechanisms were compared with rates in the literature and experimental results to improve important pathway parameters for aromatic growth.

For this task, two pathways were evaluated. The first was the addition of a vinyl radical (C_2H_3) to acetylene (C_2H_2), which is key step in a formation pathway for benzene (C_6H_6). Studying this system allowed us to confirm that we can observe ring formation in our experiment and measure the kinetics and branching ratios which describe C_4H_5/C_4H_4 formation and the yield of benzene, as shown in Figure 6.

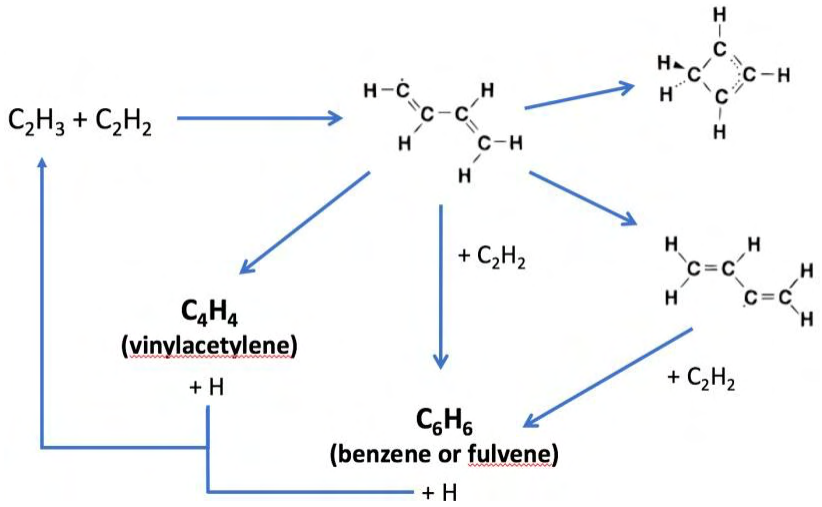

Figure 6. Formation pathways of benzene from vinyl radical and acetylene.

The second pathway explored was acetylene addition to naphthyl radicals. Although aromatic growth from naphthalene is thought to be dominated by the HACA mechanism, under experimental conditions, three-ring PAHs have generally

not been observed, thus prompting the question of what other pathways might exist that convert naphthalenes to PAHs. This question was explored with LFP/PIMS.

Milestone

The work completed for this task was documented in Deliverable 2-3, provided to the FAA on April 30, 2018.

Major Accomplishments

Results for the vinyl radical–acetylene pathway, comparing experimental time profiles with simulations, are shown in Figure 7. Kinetics calculated from LFP/PIMS were found to generally agree with the results of the RMG-generated model over a range of temperatures. Preliminary experiments for 1-naphthyl addition to C_2H_2 revealed branching between stable $C_{12}H_8$ products (e.g., acenaphthalene) and $C_{12}H_9$ adducts, as shown in Figure 8. Work to incorporate this finding into RMG is ongoing.

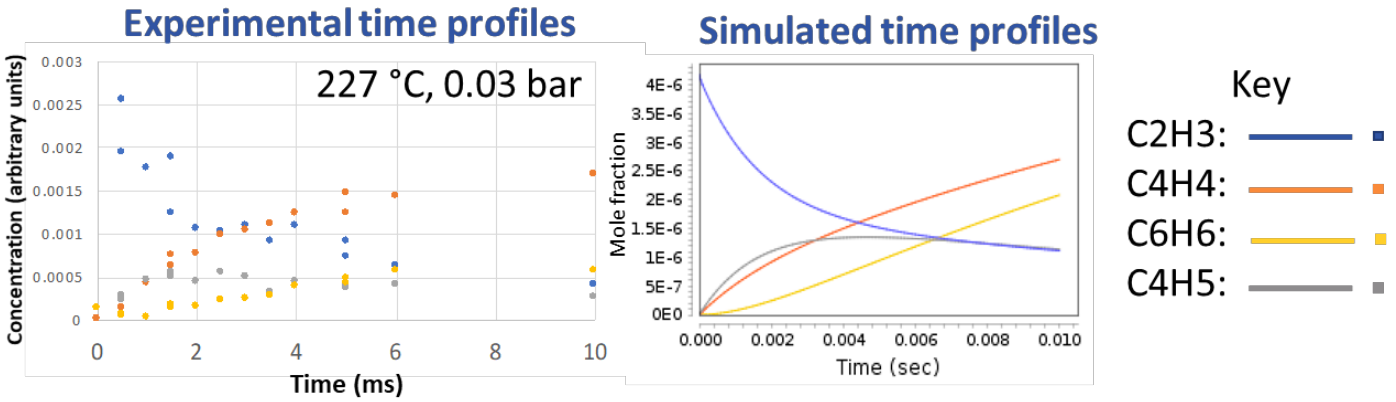

Figure 7. Comparison of experimental and simulated concentration profiles for the reaction of vinyl radical and acetylene.

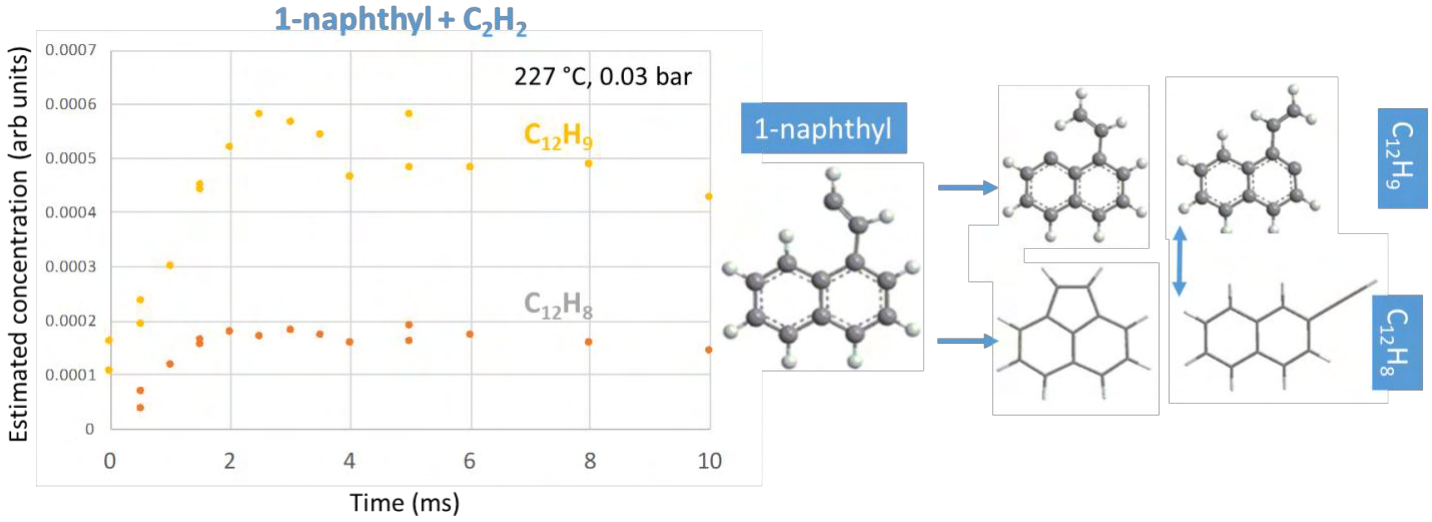

Figure 8. Experimentally-observed branching ratios between stable $C_{12}H_8$ species and $C_{12}H_9$ adducts formed by the reaction of 1-naphthyl radicals with acetylene.

Student Involvement

This work was conducted primarily by Dr. Mica Smith, a postdoctoral associate working under the supervision of Professor William Green.

Task 6 - Evaluate Changes in Emissions Resulting from Removal of Naphthalene

Massachusetts Institute of Technology

Objective

Changes to jet fuel composition, such as those achieved by the removal of naphthalene using available refining technologies, affect the chemical kinetics of the combustion process in gas turbine engines, which in turn affects the resulting emissions. The formation of black carbon (soot) from hydrocarbon fuels can be considered to occur in two stages. First, fuel components and combustion intermediates react and form PAHs. Large PAHs then act as soot nuclei, which grow as they absorb both PAH and other species, coagulate through collisions with other soot particles, carbonize, and partially oxidize (Richter & Howard, 2000). The details of the fuel composition mainly affect the first step of this process: the formation of PAHs. To enable evaluation of the sensitivity of soot emissions to fuel composition, in this task, we developed a combustor model that includes the detailed chemical kinetic pathways for the formation of (PAH) species from different fuel components and the conversion of these PAH species to soot particles or nvPM emissions. The model also provides the ability to predict changes in CO and nitrogen oxide (NO_x) emissions resulting from changes to fuel composition.

Research Approach

The aircraft engine emissions model developed herein has three main components: a soot model, an engine model, and a combustor model. The combustor model consists of a reactor network coupled with a gas-phase kinetic mechanism, which was modeled using Cantera (Goodwin et al., 2018). A soot model was added to the reactor network, and the interactions between the gas phase and the solid soot phase were modeled in detail. The altitude- and thrust-specific input conditions for the combustor were generated with the engine model, Pycaso (Python Cantera Soot). The model was used to predict emissions for a CFM56-7B/3 engine, because it is one of the most prevalent engines in the commercial fleet, and measurement data for soot emissions from this engine have been published.

Soot model

Because of the uncertainty in soot modeling in gas turbine combustors, we used a two-equation model, which captures all major soot formation and depletion processes while minimizing complexity. In a two-equation model, the soot number density (N) and mass density (M) were modeled with two equations representing the change in soot N and M in response to four soot formation and depletion steps. The standard two-equation model is based on the assumption that oxidation affects solely M and does not directly destroy soot particles. However, experiments have indicated that oxidation can destroy particles and can thus reduce N (Garo et al., 1988; Lindstedt, 1994). Therefore, an additional term was included in the number density equation to capture the effect of particle destruction through oxidation. Every change in soot mass equivalent to the average soot particle mass was assumed to also destroy a variable fraction of a particle. The resulting equations for N and M are as follows:

$$\frac{dN}{dt} = C_{\text{nuc}}\left(\frac{dN}{dt}\right)_{\text{nuc}} + C_{\text{coag}}\left(\frac{dN}{dt}\right)_{\text{coag}} + C_{\text{ox},N}\frac{N}{M}C_{\text{ox}}\left(\frac{dM}{dt}\right)_{\text{ox}}, \tag{1}$$

and

$$\frac{dM}{dt} = C_{\text{nuc}}\left(\frac{dM}{dt}\right)_{\text{nuc}} + C_{\text{sg}}\left(\frac{dM}{dt}\right)_{\text{sg}} + C_{\text{ox}}\left(\frac{dM}{dt}\right)_{\text{ox}}. \tag{2}$$

During nucleation, the inception of soot particles occurs through collisions of precursor species (Blanquart & Pitsch, 2009). These precursor species are considered to primarily consist of heavy PAH molecules (Dobbins et al., 1998; Schuetz & Frenklach, 2002). When two PAH molecules collide and stick together, they form a PAH dimer, which again increases in size through collisions with other PAH species and dimers. This growth through collisions allows for transitioning from the gas phase to the solid phase and results in the first solid incipient soot particle (Martini, 2008). PAH-PAH collision rates were considered for nucleation in the model, while PAH-soot collisions are modeled as surface growth. The nucleation rate resulting from collisions of PAH species i and j was based on the collision frequency $\beta i,j$ and is given by the following:

$$\left(\frac{dN}{dt}\right)_{\text{nuc},ij} = \frac{\gamma_i + \gamma_j}{2}\varepsilon\sqrt{\frac{8\pi k_B T}{\mu_{i,j}}}N_A^2\left(r_i + r_j\right)^2[\text{PAH}_i][\text{PAH}_j], \tag{3}$$

where ε = 2.2 is the Van der Waals enhancement factor, k_B is the Boltzmann constant, N_A is Avogadro's constant, r_i and r_j are the radii of PAH species i and j, $\mu_{i,j}$ is the reduced mass of PAH species i and j and $[\mathrm{PAH}_i]$ is the concentration of PAH species i (An et al., 2016; Atkins et al., 2018; Blanquart & Pitsch, 2009). The sticking coefficient $\gamma < 1$ was computed using the assumption that it scales with PAH mass to the fourth power (Blanquart & Pitsch, 2009). The PAH species were chosen such that no direct pathways from species in the fuel surrogates to soot mass through nucleation exist, as these pathways might result in an overestimation of sensitivities to fuel composition. The total nucleation rate was calculated by taking the sum over all the PAH species in the gas-phase mechanism.

Nucleation is followed by surface growth and coagulation. During surface growth, the soot particles grow in size and mass, because of the adsorption of gas phase molecules, mainly acetylene (Omidvarborna et al., 2015). Growth rates have been found to be much higher than nucleation rates, and most of the soot mass is thought to form during this step in the process (Martini, 2008). Here, two types of surface growth mechanisms were implemented. The first was based on an assumption of surface growth solely by acetylene, whereas the second also included surface growth through condensation of PAH species on the soot surface. To include surface growth through the adsorption of PAH species, the surface growth source term was expanded with an additional term based on the collision frequency of soot particles with PAH species i, given by:

$$\left(\frac{dM}{dt}\right)_{\mathrm{sg,PAH}} = \sum_{i=1}^{L} n_{\mathrm{C},i} W_{\mathrm{C}} \frac{\gamma_i + \gamma_{soot}}{2} \varepsilon \sqrt{\frac{8\pi k_B T}{\mu_{\mathrm{soot},i}}} \left(r_i + \frac{d_p}{2}\right)^2 [\mathrm{PAH}_i] N. \tag{4}$$

Because this term is similar to the nucleation term, it was scaled with C_{nuc} instead of C_{sg}.

During coagulation, soot particles grow further through particle-particle collisions (Blanquart & Pitsch, 2009; Omidvarborna et al., 2015). The total number of soot particles decreases during coagulation, whereas the total mass across all particles remains constant. The implemented coagulation mechanism was based on the collision of two spherical particles with a collision rate, as defined by Puri et al. (1993). The resulting source term for the number density equation is given by:

$$\left(\frac{dN}{dt}\right)_{\mathrm{coag}} = -K_{\mathrm{coag}} \sqrt{\frac{24 R_u T}{\rho_{\mathrm{soot}} N_A}} \sqrt{d_p} N^2, \tag{5}$$

where ρ_{soot} was assumed to be equal to 2000 kg/m^3 and K_{coag} is a constant ranging between 1 and 9 in literature (Brookes & Moss, 1999; Wen et al., 2003).

In contrast to the previous three steps, soot is destroyed during oxidation. Oxidation significantly reduces the amount of soot and measurements have suggested that most of the soot formed at the start of the combustion process is oxidized before reaching the combustor exit (Toone, 1968). Carbon and hydrogen atoms are removed from the soot agglomerates by reactions with primarily diatomic oxygen (O_2), hydroxyl radicals (OH) and atomic oxygen (O) (Louloudi, 2003; Neoh et al., 1981). Their respective contributions to the oxidation source term (Guo et al., 2016; Martini, 2008; Schiener & Lindstedt, 2018) are given by:

$$\left(\frac{dM}{dt}\right)_{\mathrm{ox},O_2} = -745.88 \eta_{O_2} W_{\mathrm{C}} \sqrt{T} \exp\left(-\frac{19{,}680}{T}\right) [O_2] A_s, \tag{6}$$

and

$$\left(\frac{dM}{dt}\right)_{\mathrm{ox,OH}} = -\eta_{\mathrm{OH}} W_{\mathrm{C}} \sqrt{T} [\mathrm{OH}] A_{s,} \tag{7}$$

and

$$\left(\frac{dM}{dt}\right)_{\mathrm{ox,O}} = -1.82 \eta_{\mathrm{O}} W_{\mathrm{C}} \sqrt{T} [\mathrm{O}] A_s, \tag{8}$$

where the collision efficiencies for O_2 and O ($\eta_{O_2}$and η_{O}) are assumed to be unity (Mueller et al., 2009; Wen et al., 2003). For oxidation through OH, collision efficiency values ranging from 0.01 to 0.65 have been proposed (Fenimore & Jones,

1967; Ghiassi et al., 2017; Guo et al., 2016; Haudiquert et al., 1997; Neoh et al., 1981; Puri et al., 1994; Richter et al., 2005; Schiener & Lindstedt, 2018). We used a value of 0.13, determined by Neoh et al. (1981), as the baseline value in this model.

Engine model

The combustor inlet temperature (T_3) and pressure (P_3), as well as the mass flows of fuel ($\dot{m}_{\mathrm{f\,uel}}$) and air ($\dot{m}_{\mathrm{air}}$) entering the combustor were computed using a detailed engine model of the CFM56-7B engine. The engine model is developed using the Numerical Propulsion System Software (NPSS) and matches the fuel flows, thrust levels and pressure ratios from the International Civil Aviation Organization (ICAO) engine emissions databank (EDB) within 5%. The temperature of the gas-phase mixture entering the combustor was corrected for vaporization of the fuel by adjusting the specific enthalpy of the gas-fuel mixture as follows:

$$h_{\mathrm{mix}} = \frac{1}{\dot{m}_{\mathrm{air}}}\left[\dot{m}_{\mathrm{air}} h_{\mathrm{air},P_3T_3} + \dot{m}_{\mathrm{fuel}} h_{\mathrm{fuel},P_3T_3} - \dot{m}_{\mathrm{fuel}}(L + \Delta h)\right], \tag{9}$$

where L represents the enthalpy of vaporization at standard conditions (T =298.15 K and P = 101,325 Pa), h is the specific enthalpy and Δh is the change in specific enthalpy going from standard conditions to T_3 and P_3. $\dot{m}_{\mathrm{fuel}}$ and $\dot{m}_{\mathrm{air}}$ are the mass flow rates of fuel and air, respectively.

Combustor model

The combustor model developed for this project represents a rich-burn quick-mix Lean-Burn (RQL) combustor. Figure 9 shows a schematic overview of the model. The model is divided into two parts: the primary zone and the secondary zone. In the primary zone, air and fuel are mixed at a certain equivalence ratio. Quenching then occurs at the start of the secondary zone through to the addition of secondary air in the slow and fast mixing zones. In the second part of the secondary zone, dilution air is added to represent the lean burn zone. Because NO_x, CO and soot reactions have been found to be quenched at the end of the secondary zone, the turbine was not modeled. The gas phase chemistry inside the combustor model was modeled using a kinetic mechanism that determines the structure of the flame and specifies the species profile (Appel et al., 2000). A high temperature kinetic mechanism for transportation fuels was coupled with a NO_x mechanism, thus resulting in a chemical mechanism consisting of 218 species and 7047 reactions (Ranzi et al., 2012, 2014, 2015).

The combustor model can be used to represent different (RQL) combustors. To represent a specific combustor design, combustor model parameters were calibrated by using emissions data from the EDB for an engine containing that specific combustor. Because the combustor model can be considered a "black box" function, and obtaining a (numerical) gradient is computationally expensive, gradient-free optimization was used to calibrate the model parameters. More specifically, the DIvided RECTangles (DIRECT) method was applied (Finkel, 2003; Hicken et al., 2012; Jones, 2009).

Milestone

The combined combustor, soot, and engine model described above were implemented, then used to explore the impacts of different jet fuel compositions on NO_x, CO, and soot emissions.

Major Accomplishments

Model validation

Eight different soot model configurations (C1 – C8) were developed. Each configuration consists of a different set of reaction rate coefficients and/or soot mechanisms. These eight configurations were selected to capture a range of soot mechanisms in literature and to quantify the impact and behavior of each step of the soot formation process. The performance of the configurations against measurements for both emissions index (EI) mass and number is summarized in Figure 10. Starting with EI soot mass, two clusters of configurations are visible. Configurations 1-5 capture the trends in the validation data for thrust levels >= 30%. On the other hand, configurations 6-8 capture the trend in the data for thrust settings larger than approximately 75% but underpredict soot mass emissions thrust settings lower than 75%. For soot number EI, the models all capture the trend in the validation data of decreasing number EI with increasing thrust between approximately 60% and 100% thrust. Configurations 4,5, and 6 also capture the 30% thrust point, whereas configurations 1,2,7, and 8 underpredict soot number at this thrust setting, while configuration 3 overpredicts it.

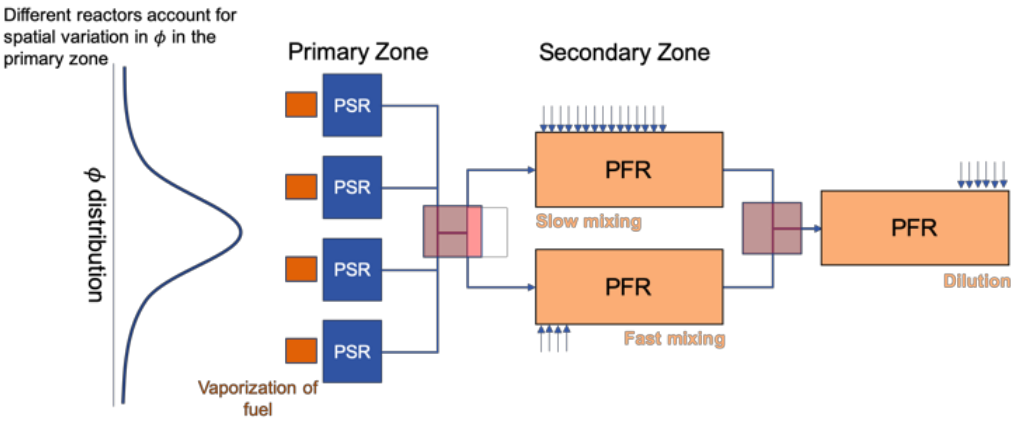

Figure 9. Schematic overview of the combustor model. Multiple well-stirred reactors (WSR) are used in the primary zone. The secondary zone uses a combination of plug flow reactors (PFR) to simulate different mixing times. The arrows represent secondary and dilution air entering the combustor.

We found primary zone soot mass formation peaks at $\varphi \approx 2.3$, where the EI soot was approximately seven times higher than that at $\varphi \approx 3.0$ and $\varphi \approx 2.0$. In contrast, the soot number increased with the equivalence ratio, and peak EI soot number values were observed in the richest reactors. This difference can be explained by the PAH concentration being the limiting factor for nucleation (soot number), whereas temperature and C_2H_2 concentration are the limiting factors for soot mass (surface growth).

To validate the model's ability to predict changes in soot emissions in response to changing fuel compositions, we simulated a subset of the experiments conducted by Brem et al. (2015), in which soot emissions were measured for two fuel blends with differing naphthalene and aromatic content. The soot predictions of each of the model configurations for two versions of each of the five surrogates were evaluated. The content of total aromatics (% v/v), naphthalene (% v/v), and hydrogen of these two fuels matched the values used in experiments by Brem et al. (2015). The resulting changes in EI soot mass and

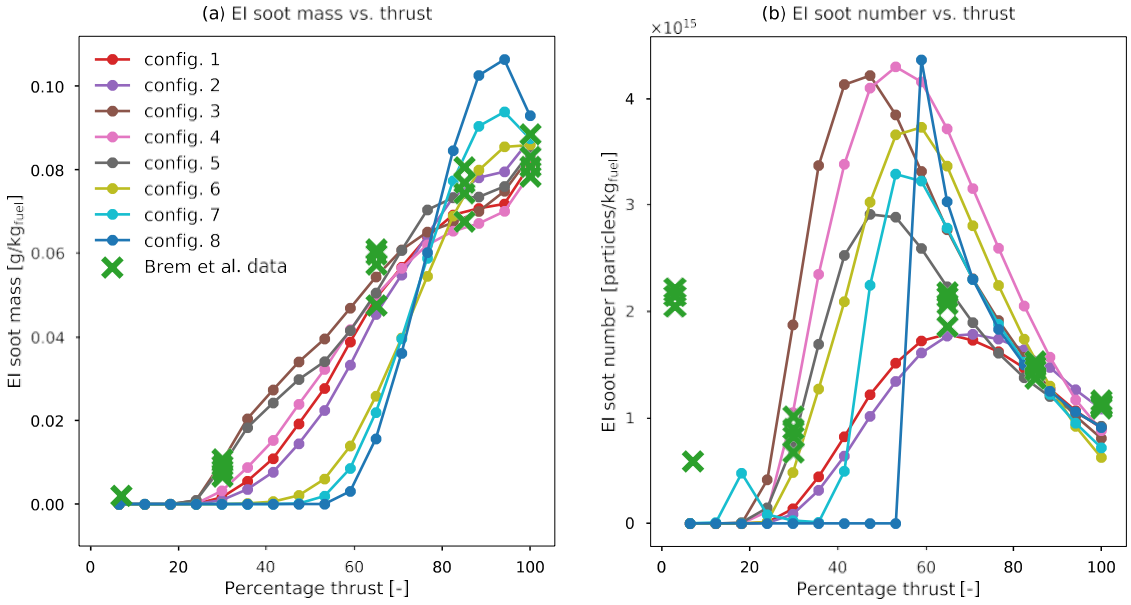

Figure 10. Comparison of EI soot (a) mass and (b) number with validation data (surrogate 4).

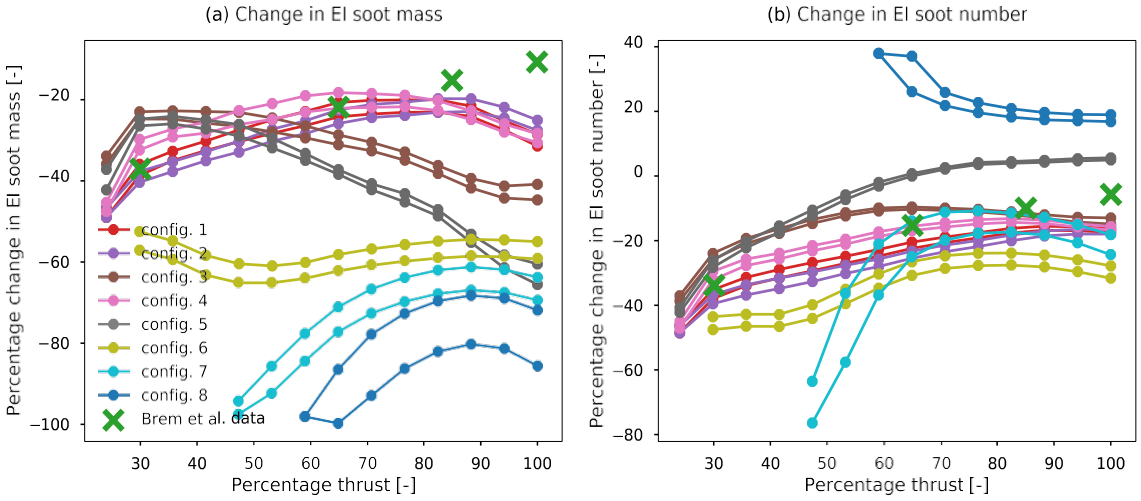

Figure 11. Comparison of model predictions with experimental data by Brem et al. (2015). Percentage change in EI soot (a) mass and (b) number for all eight configurations.

number are shown in Figure 11. The three configurations using the HACA mechanisms showed large discrepancies for both soot mass and number. The five other configurations could be grouped based on their values for C_{coag} and $C_{ox,N}$. The three configurations (1, 2, and 4) with relatively low coagulation factors (< 30) and relatively large $C_{ox,N}$ values (> 0.65) matched the soot mass data from Brem et al. (2015) within 5 percentage points (p.p.) at 30% and 65% thrust, 8 p.p. at 85% thrust and 18 p.p. at 100% thrust, and within 15 p.p. of the soot number data for all thrust conditions. When increasing the coagulation factor and decreasing $C_{ox,N}$ (configurations 3 and 5), these differences grew to a maximum of 51 p.p. at 100% thrust for configuration 5. A possible explanation for the relatively large discrepancies at high thrust for the configuration using high coagulation factors is that these configurations rely on a large N in the PZ to increase the average particle size (and thus the M/A_s ratio). When reducing the naphthalene content of the fuel, less nucleation occurs, and the soot number density decreases. Consequently, coagulation is decreased and M/A_s is increased thus leading to more oxidation in the secondary zone. In contrast, configurations relying on $C_{ox,N}$ to reduce N are relatively less affected by a decreasing N. Because of their superior performance with respect to the validation data, configurations 1, 2, and 4 were selected to assess the sensitivity of soot to naphthalene removal and biofuels in the subsequent analysis of fuel composition effects.

Effects of fuel composition

Figure 12 shows the computed ranges of soot mass and number emissions reductions associated with naphthalene removal through extractive distillation and hydrotreating. These ranges represent both variations in the three soot model configurations as well as the five baseline fuel compositions. The mean reductions in EI mass were approximately 20 p.p. higher for extractive distillation than for hydrotreating. For EI soot number, the differences between the means of the two methods ranged from 12 p.p. at 100% thrust to 28 p.p. at 30% thrust. These differences are explained by tetralin, the product of hydrotreating naphthalene, being an aromatic species and having a relatively short pathway to becoming a PAH species during combustion. Reductions in mass are predicted to be larger than those in number (for >35% thrust), in agreement with the literature (Brem et al., 2015; Speth et al., 2015).

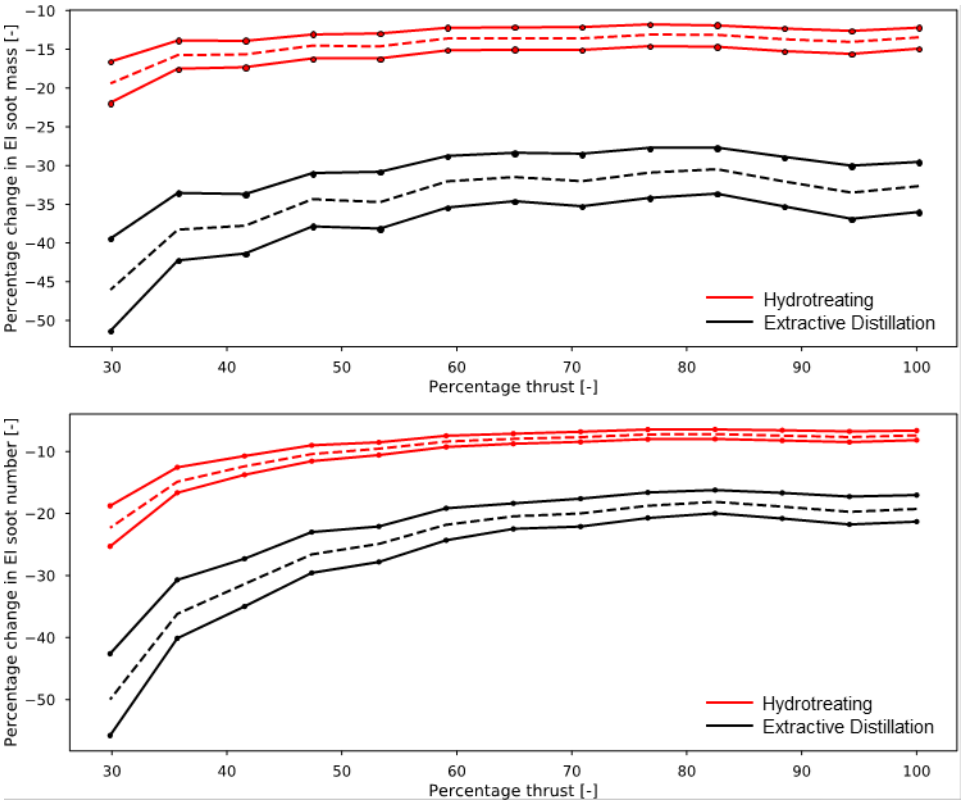

Figure 12. Ranges of predicted effects of naphthalene removal from jet fuel by hydrotreating (red) and extractive distillation (black) on EI soot (a) mass and (b) number emissions indices. The dashed lines represent the means of the prediction ranges, which capture variations in three different soot configurations and five different surrogates.

Furthermore, particularly for number emissions, reductions increase with decreasing thrust. This effect has also been observed in experiments in the literature (Brem et al., 2015; Corporan et al., 2007; Naegeli & Moses, 2015; Speth et al., 2015). We found that the increasing change in soot emissions with decreasing thrust can be explained by two main factors. The first factor is that sensitivity to fuel composition increases with decreasing PZ equivalence ratio. The changes in EI soot mass and number due to naphthalene removal were found to be approximately 1.5 and 2–3 times higher at φ=2.2 compared to φ=3.0, respectively. The lower the thrust setting, the lower the primary zone equivalence ratio(s), and thus the higher the sensitivity to fuel composition. The second factor is that for a given φ, the reductions in both soot mass and number increase with decreasing thrust. This is explained by the temperature difference between the thrust conditions. Higher temperatures at higher thrust settings make the reactor more resilient to changes in naphthalene concentrations.

Figure 13 shows the predicted effects of using 20%, 50%, and 100% biofuel blends on soot emissions. As expected, the mean reductions increase with increasing biofuel fraction and decreasing thrust. The predicted reductions for soot mass range from 17%, 37%, and 55% at 100% thrust to 25%, 56%, and 92% at 30% thrust. For soot number, the mean reductions at 100% thrust are 11%, 26%, and 51%, as compared with reductions of 24%, 56%, and 92% at 30% thrust.

The effects of using 20%, 50%, and 100% biofuel blends on NO_x and CO emissions are shown in Figure 14. The model predicts the mean reductions in NO_x emissions of 2%, 5%, and 10% and those in CO emissions of 1%, 2%, and 5% for the three blends, respectively. The sharp drop in CO at the lowest thrust setting is a consequence of the finite number of reactors in the model; the corresponding CO values were therefore not considered. This sharp drop in CO occurs because the leanest reactor blows out for the standard surrogate but does not do so for the 50% and 100% biofuel blends, thus leading to an increase in SZ mixing temperature and consequently CO depletion.

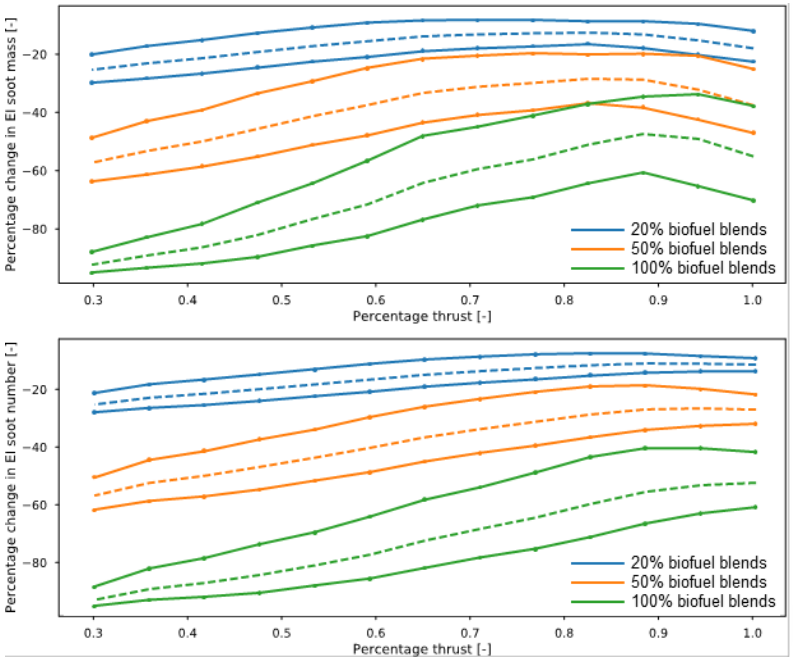

Figure 13. Effects of using 20% (blue), 50% (orange), and 50% (green) biofuel blends on EI soot (a) mass and (b) number. The dashed lines represent the means of the prediction ranges, which capture variations in three soot mechanisms and five surrogates.

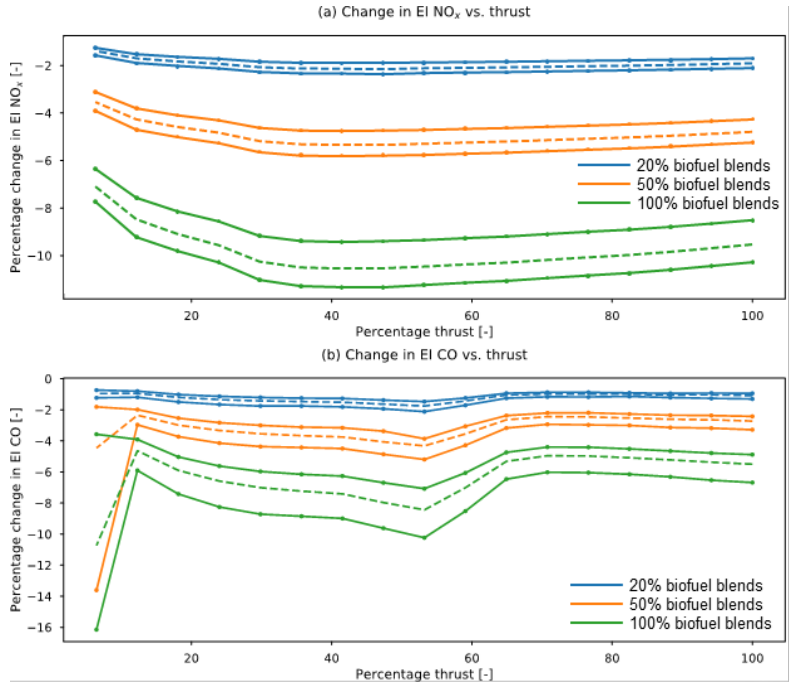

Figure 14. Effects of using 20% (blue), 50% (orange), and 100% (green) biofuel blends on (a) NO_x and (b) CO emissions. The dashed lines represent the means of the prediction ranges, which capture variations in five surrogates.

Publications

Brink, L. (2020). Modeling the impact of fuel composition on aircraft engine NO_x, CO and soot emissions [S.M. thesis, Massachusetts Institute of Technology]. DSpace@MIT. https://hdl.handle.net/1721.1/129181

Outreach Efforts

- ASCENT advisory board presentations (October 2018, October 2019, and March 2020)
- Presentations at the Aviation Emissions Characterization (AEC) Roadmap Annual Meeting (June 2017 and May 2020)

Student Involvement

This task was conducted primarily by Lukas Brink, working directly with Professor Steven Barrett and Dr. Raymond Speth. Mr. Brink graduated with a Master of Science degree in 2020.

References

An, Y., Li, X., Teng, S., Wang, K., Pei, Y., Qin, J., & Zhao, H. (2016). Development of a soot particle model with PAHs as precursors through simulations and experiments. Fuel, *179*, 246–257. https://doi.org/10.1016/j.fuel.2016.03.100

Appel, J., Bockhorn, H., & Frenklach, M. (2000). Kinetic modeling of soot formation with detailed chemistry and physics: Laminar premixed flames of C_2 hydrocarbons. Combustion and Flame, *121*(1–2), 122–136.

Atkins, P. W., De Paula, J., & Keeler, J. (2018). *Atkins' physical chemistry*. Oxford University Press.

Blanquart, G., & Pitsch, H. (2009). A joint volume-surface-hydrogen multi-variate model for soot formation. Combustion Generated Gine Carbonaceous Particles, 437–463.

Brem, B. T., Durdina, L., Siegerist, F., Beyerle, P., Bruderer, K., Rindlisbacher, T., Rocci-Denis, S., Andac, M. G., Zelina, J., Penanhoat, O., & Wang, J. (2015). Effects of fuel aromatic content on nonvolatile particulate emissions of an in-production aircraft gas turbine. Environmental Science and Technology, *49*, 13149–13157.

Brookes, S. J., & Moss, J. B. (1999). Predictions of soot and thermal radiation properties in confined turbulent jet diffusion flames. Combustion and Flame, *116*(4), 486–503. https://doi.org/10.1016/S0010-2180(98)00056-X

Corporan, E., DeWitt, M. J., Belovich, V., Pawlik, R., Lynch, A. C., Gord, J. R., & Meyer, T. R. (2007). Emissions characteristics of a turbine engine and research combustor burning a Fischer–Tropsch jet fuel. Energy and Fuels, *21*(5), 2615–2626. https://doi.org/10.1021/ef070015j

Dobbins, R. A., Fletcher, R. A., & Chang, H.-C. (1998). The evolution of soot precursor particles in a diffusion flame. Combustion and Flame, *115*(3), 285–298. https://doi.org/10.1016/S0010-2180(98)00010-8

Fenimore, C. P., & Jones, G. W. (1967). Oxidation of soot by hydroxyl radicals. The Journal of Physical Chemistry, *71*(3), 593–597. https://doi.org/10.1021/j100862a021

Finkel, D. (2003). *DIRECT optimization algorithm user guide*. North Carolina State University Center for Research in Scientific Computation.

Garo, A., Lahaye, J., & Prado, G. (1988). Mechanisms of formation and destruction of soot particles in a laminar methane-air diffusion flame. Symposium (International) on Combustion, *21*(1), 1023–1031. https://doi.org/10.1016/S0082- 0784(88)80333-3

Ghiassi, H., Lignell, D., & Lighty, J. S. (2017). Soot oxidation by OH: Theory development, model, and experimental validation. Energy and Fuels, *31*(3), 2236–2245. https://doi.org/10.1021/acs.energyfuels.6b02193

Goodwin, D. G., Speth, R. L., Moffat, H. K., & Weber, B. W. (2018). Cantera: An object-oriented software toolkit for chemical kinetics, thermodynamics, and transport processes (2.4.0) [Computer software]. https://www.cantera.org.

Guo, H., Anderson, P. M., & Sunderland, P. B. (2016). Optimized rate expressions for soot oxidation by OH and O2. Fuel, *172*, 248–252. https://doi.org/10.1016/j.fuel.2016.01.030

Haudiquert, M., Cessou, A., Stepowski, D., & Coppalle, A. (1997). OH and soot concentration measurements in a high-temperature laminar diffusion flame. Combustion and Flame, *111*(4), 338–349. https://doi.org/10.1016/S0010- 2180(97)00003-5

Hicken, J., Alonso, J., & Farhat, C. (2012). Chapter 6: Gradient-free optimization. In *Introduction to multidisciplinary design optimization* (pp. 133-161). Stanford University.

Jones, D. R. (2009). Direct global optimization algorithm. Encyclopedia of Optimization, *1*(1), 431–440.

Lindstedt, P. R. (1994). Simplified soot nucleation and surface growth steps for non-premixed flames. In H. Bockhorn (Ed.), *Soot formation in combustion: Mechanisms and models* (pp. 417–441). Springer. https://doi.org/10.1007/978-3-642-85167-4_24

Louloudi, S. (2003). *Transported probability density function: Modelling of turbulent jet flames*. Imperial College London (University of London).

Martini, B. (2008). *Development and assessment of a soot emissions model for aircraft gas turbine engines* [S. M. thesis, Massachusetts Institute of Technology]. DSpace@MIT. https://dspace.mit.edu/handle/1721.1/45256

Mueller, M. E., Blanquart, G., & Pitsch, H. (2009). Hybrid method of moments for modeling soot formation and growth. Combustion and Flame, *156*(6), 1143–1155. https://doi.org/10.1016/j.combustflame.2009.01.025

Naegeli, D. W., & Moses, C. A. (2015, April 17). Effect of fuel molecular structure on soot formation in gas turbine engines [Presentation]. ASME 1980 International Gas Turbine Conference and Products Show. https://doi.org/10.1115/80-GT-62

Neoh, K. G., Howard, J. B., & Sarofim, A. F. (1981). Soot oxidation in flames. In D. C. Siegla & G. W. Smith (Eds.), *Particulate carbon: Formation during combustion* (pp. 261–282). Springer US. https://doi.org/10.1007/978-1-4757-6137-5_9

Omidvarborna, H., Kumar, A., & Kim, D.-S. (2015). Recent studies on soot modeling for diesel combustion. Renewable and Sustainable Energy Reviews, *48*, 635–647. https://doi.org/10.1016/j.rser.2015.04.019

Puri, R., Richardson, T. F., Santoro, R. J., & Dobbins, R. A. (1993). Aerosol dynamic processes of soot aggregates in a laminar ethene diffusion flame. Combustion and Flame, *92*(3), 320–333.

Puri, R., Santoro, R. J., & Smyth, K. C. (1994). Oxidation of soot and carbon monoxide in hydrocarbon diffusion flames. Combustion and Flame, *97*, 125–144.

Ranzi, E., Cavallotti, C., Cuoci, A., Frassoldati, A., Pelucchi, M., & Faravelli, T. (2015). New reaction classes in the kinetic modeling of low temperature oxidation of n-alkanes. Combustion and Flame, *162*(5), 1679–1691. https://doi.org/10.1016/j.combustflame.2014.11.030

Ranzi, E., Frassoldati, A., Grana, R., Cuoci, A., Faravelli, T., Kelley, A. P., & Law, C. K. (2012). Hierarchical and comparative kinetic modeling of laminar flame speeds of hydrocarbon and oxygenated fuels. Progress in Energy and Combustion Science, *38*(4), 468–501. https://doi.org/10.1016/j.pecs.2012.03.004

Ranzi, E., Frassoldati, A., Stagni, A., Pelucchi, M., Cuoci, A., & Faravelli, T. (2014). Reduced kinetic schemes of complex reaction systems: Fossil and biomass-derived transportation fuels. International Journal of Chemical Kinetics, *46*(9), 512–542. https://doi.org/10.1002/kin.20867

Richter, H., Granata, S., Green, W. H., & Howard, J. B. (2005). Detailed modeling of PAH and soot formation in a laminar premixed benzene/oxygen/argon low-pressure flame. Proceedings of the Combustion Institute, *30*(1), 1397–1405. https://doi.org/10.1016/j.proci.2004.08.088

Schiener, M. A., & Lindstedt, R. P. (2018). Joint-scalar transported PDF modelling of soot in a turbulent non-premixed natural gas flame. Combustion Theory and Modelling, *22*(6), 1134–1175. https://doi.org/10.1080/13647830.2018.1472391

Schuetz, C. A., & Frenklach, M. (2002). Nucleation of soot: Molecular dynamics simulations of pyrene dimerization. Proceedings of the Combustion Institute, *29*(2), 2307–2314. https://doi.org/10.1016/S1540-7489(02)80281-4

Speth, R. L., Rojo, C., Malina, R., & Barrett, S. R. H. (2015). Black carbon emissions reductions from combustion of alternative jet fuels. Atmospheric Environment, *105*, 37–42. https://doi.org/10.1016/j.atmosenv.2015.01.040

Toone, B. (1968). A review of aero engine smoke emission. In I. E. Smith (Ed.), *Combustion in advanced gas turbine systems* (pp. 271–296). Pergamon. https://doi.org/10.1016/B978-0-08-013275-4.50019-2

Wen, Z., Yun, S., Thomson, M. J., & Lightstone, M. F. (2003). Modeling soot formation in turbulent kerosene/air jet diffusion flames. Combustion and Flame, *135*(3), 323–340. https://doi.org/10.1016/S0010-2180(03)00179-2

Task 7 - Calculate Air Quality and Climate Impacts of Naphthalene Removal

Massachusetts Institute of Technology

Objective

The objective of this task was to calculate the air quality and climate impacts of a policy in which naphthalene is removed from jet fuel used in the United States.

Research Approach

The air quality effects of changes in aircraft PM emissions were evaluated by using the GEOS-Chem adjoint model, which we previously used for assessing the health impacts of emissions (Dedoussi & Barrett, 2014). The use of an adjoint model, a computationally efficient approach to calculating the sensitivity of an aggregate objective function (e.g., population exposure to $PM_{2.5}$), enables evaluation of a range of scenarios in a single run, thus allowing for incorporation of upstream uncertainty in the emissions indices for different species. The PM exposure calculated by using GEOS-Chem included both the effects of changes in black carbon emissions and changes due to sulfur reductions that accompany the removal of naphthalenes (in the case in which hydrotreating is used to remove naphthalenes). The spatial patterns of emissions of nvPM, and sulfur compounds were taken from the 2015 inventory from the Aviation Environmental Design Tool (AEDT).

Climate impacts of naphthalene removal include contributions at both the fuel production and fuel consumption stages.

The additional refinery processing required to reduce or remove naphthalene requires process fuel, steam, electricity, and, in the case of hydrotreating, hydrogen production. The greenhouse gas (GHG) emissions associated with each of these processes increase life-cycle jet fuel GHG emissions. Using the results calculated as part of the refinery modeling work conducted in the previous project year, we found that the GHG emissions associated with naphthalene removal were 135 g CO_2e per kg fuel for hydrotreating and 144 g CO_2e per kg fuel for extractive distillation.

The consumption of reduced-naphthalene fuel decreases RF from aviation black carbon, and reductions in sulfur content decrease the cooling effect of sulfates (Mahashabde et al., 2011). Contrail impacts are estimated according to studies on the impact of reducing the number of ice nuclei available for contrail formation. Caiazzo et al. (2017) have found that decreasing ice nuclei by 67% (an amount representative of a fully paraffinic biofuel) reduces contrail RF by <13%. Burkhardt et al. (2018) have found that reducing ice nuclei by 50% reduces contrail RF by ~20%. Here, the reductions in contrail RF found in these studies were scaled by the estimated reduction in nvPM emissions from naphthalene removal.

The combined climate impacts of these effects were evaluated by using the APMT-Impacts Climate model, a policy-oriented rapid assessment tool that provides probabilistic estimates of climate impacts.

Milestone

The work completed for this task was documented in Deliverable 2-4, provided to the FAA on May 31, 2018.

Major Accomplishments

On the basis of a literature review of nvPM emissions measurements from engines using fuels with varying levels of naphthalene (Brem et al., 2015; DeWitt et al., 2008), we estimated the potential range of reduction in nvPM emissions associated with 95% naphthalene removal to be 15–40%, or 5.0–12.5 mg nvPM per kg fuel. Monetized climate impacts for the different climate forcing pathways are summarized in Table 2, presented on a cents-per-gallon basis, with both median values and a range indicating the 90% CI. Monetized air quality impacts of naphthalene removal are similarly summarized in Table 3.

Table 2. Monetized climate benefits of naphthalene removal.

Impact Pathway	Impact (¢/gallon)
Black carbon RF (15% nvPM reduction)	0.09 (90% CI: 0.01 to 0.23)
Black carbon RF (40% nvPM reduction)	0.23 (90% CI: 0.04 to 0.61)
Contrail RF (15% nvPM reduction)	1.06 (90% CI: 0.30 to 2.59)
Contrail RF (40% nvPM reduction)	2.77 (90% CI: 0.77 to 6.89)
Hydrotreating CO_2 emissions	−1.82 (90% CI: −0.30 to −4.70)
Extractive distillation CO_2 emissions	−1.89 (90% CI: −0.31 to −5.01)
Sulfate aerosol (hydrotreating only)	−4.17 (90% CI: −0.61 to −11.23)

Table 3. Monetized air quality benefits of naphthalene removal.

Impact Pathway	Impact (¢/gallon)
nvPM emissions (15% nvPM reduction)	0.04 (90% CI: 0.02 to 0.06)
nvPM emissions (40% nvPM reduction)	0.11 (90% CI: 0.06 to 0.16)
Sulfur emissions (hydrotreating only)	1.92 (90% CI: 1.04 to 2.76)

Outreach Efforts

- ASCENT advisory board presentations (October 2018 and October 2019)
- Presentation at the CAEP/12-WG3/2 meeting (October 2019) titled “Economic and Environmental Assessment of Jet Fuel Naphthalene Removal”

Student Involvement

This task was conducted primarily by Drew Weibel, a Master's student in the Laboratory for Aviation and the Environment, working directly with Professor Steven Barrett and Dr. Raymond Speth.

References

Brem, B. T., Durdina, L., Siegerist, F., Beyerle, P., Bruderer, K., Rindlisbacher, T., Rocci-Denis, S., Andac, M. G., Zelina, J., Penanhoat, O., & Wang, J. (2015). Effects of fuel aromatic content on nonvolatile particulate emissions of an in-production aircraft gas turbine. Environmental Science and Technology, *49*, 13149–13157.

Burkhardt, U., Bock, L., & Bier, A. (2018). Mitigating the contrail cirrus climate impact by reducing aircraft soot number emissions. Climate and Atmospheric Science, *1*, 37.

Caiazzo, F., Agarwal, A., Speth, R. L., & Barrett, S. R. H. (2017). Impact of biofuels on contrail warming. Environmental Research Letters, *12*, 114013.

Dedoussi, I. C., & Barrett, S. R. H. (2014). Air pollution and early deaths in the United States. Part II: Attribution of PM2.5 exposure to emissions species, time, location and sector. Atmospheric Environment, *99*, 610–617.

DeWitt, M. J., Corporan, E., Graham, J. & Minus, D. (2008). Effects of aromatic type and concentration in Fischer–Tropsch fuel on emissions production and material compatibility. Energy and Fuels, *22*, 2411–2418.

Mahashabde, A., Wolfe, P., Ashok, A., Dorbian, C., He, Q., Fan, A., Lukachko, S., Mozdzanowska, A., Wollersheim, C., Barrett, S. R. H., Locke, M., & Waitz, I. A. (2011). Assessing the environmental impacts of aircraft noise and emissions. Progress in Aerospace Sciences, *47*, 15–52.

Punger, E. M., & West, J. J. (2013). The effect of grid resolution on estimates of the burden of ozone and fine particulate matter on premature mortality in the USA. Air Quality, Atmosphere & Health, *6*, 563–573.

Task 8 · Conduct Integrated Cost-Benefit Analysis of Impacts of Naphthalene Removal in the United States

Massachusetts Institute of Technology

Objective

The objective of this task was to produce an integrated cost–benefit analysis of naphthalene removal in the United States, accounting for the additional refining cost as well as the air quality and climate impacts.

Research Approach

The overall cost–benefit assessment of naphthalene removal includes fuel production costs, air quality benefits, and climate impacts from fuel production and fuel consumption. Fuel production costs were evaluated in tasks that were completed in previous project years. Air quality benefits and non-contrail climate impacts were calculated per unit reduction in nvPM mass and number emissions, based on the results of Grobler et al. (2019). These impacts were then scaled by using the emissions reductions determined in the results of Task 1. Contrail impacts were estimated on the basis of contrail modeling studies investigating the effects of reductions in the soot number emissions index (Caiazzo et al., 2017; Bier & Burkhardt, 2019). Finally, all effects were placed on a common monetized basis to compare different naphthalene removal scenarios. We considered uncertainties in the assessment of each component and used these uncertainties to compute the likelihood of a net benefit for different scenarios.

Milestone

The work completed for this task was documented in Deliverable 2-5, provided to the FAA on July 31, 2018.

Major Accomplishments

The processing costs, air quality benefits, and climate impacts of naphthalene removal were converted to a common basis of cents per liter, as presented in Table 4. The results indicate that the benefits of widespread naphthalene removal are outweighed by the costs of processing the fuel and the CO_2 emissions associated with that processing.

Table 4. Costs (positive) and benefits (negative) of naphthalene removal.

	Component	Hydrotreatment (¢/liter)		Extractive Distillation (¢/liter)	
		Median	95% CI	Median	95% CI
Processing	Refinery	2.4	2.0 to 2.7	1.7	1.5 to 2.0
Air Quality	nvPM	−0.004	0 to −0.01	−0.009	0 to −0.03
	Fuel sulfur	−0.51	−0.28 to −0.73	0	
Climate	nvPM	−0.02	0 to −0.04	−0.04	−0.01 to −0.09
	Fuel sulfur	1.06	0.15 to 2.85	0	
	Contrails	−0.16	−0.04 to −0.44	−0.38	−0.09 to −1.0
	Refinery CO_2	0.46	0.08 to 1.19	0.48	0.08 to 1.27
Total		**3.2**	**2.2 to 4.7**	**1.8**	**1.0 to 2.5**

For hydrotreatment, the climate impacts of the refinery CO_2 emissions exceed the expected air quality and climate benefits associated with the reduction in soot emissions. Furthermore, the NPV of the climate warming associated with sulfur removal is greater than the NPV of the reduced air-quality-related damages. For extractive distillation, the median air quality and climate benefits are approximately equal to the societal cost of the refinery CO_2 emissions. In addition to these environmental costs, the costs associated with processing jet fuel in the refinery must also be considered. These results suggest that, in the absence of a strong contrail effect, naphthalene removal on a nationwide basis is unlikely to be cost beneficial using either extractive distillation or hydrotreatment. However, it may be possible that naphthalene removal could be beneficial under certain circumstances, e.g., if applied to fuels used at individual airports with particular air quality concerns, or if used at times in locations where the formation of net warming contrails is most likely.

Outreach Efforts

- ASCENT advisory board presentations (April 2017, April 2018, October 2018, and October 2019)
- Presentation at the CAEP/12-WG3/2 meeting (October 2019) titled "Economic and Environmental Assessment of Jet Fuel Naphthalene Removal"
- Presentation at the Aviation Emissions Characterization (AEC) Roadmap annual meeting (May 2020)

Student Involvement

This task was conducted primarily by Drew Weibel, a Master's student in the Laboratory for Aviation and the Environment, working directly with Professor Steven Barrett and Dr. Raymond Speth.

References

Bier, A., & Burkhardt, U. (2019). Variability in contrail ice nucleation and its dependence on soot number emissions. Journal of Geophysical Research: Atmospheres, *124*(6), 3384–3400. https://doi.org/10.1029/2018JD029155

Caiazzo, F., Agarwal, A., Speth, R. L., & Barrett, S. R. H. (2017). Impact of biofuels on contrail warming. Environmental Research Letters, *12*(11), 114013. https://doi.org/10.1088/1748-9326/aa893b

Grobler, C., Wolfe, P. J., Dasadhikari, K., Dedoussi, I. C., Allroggen, F., Speth, R. L., Eastham, S. D., Agarwal, A., Staples, M. D., Sabnis, J., & Barrett, S. R. H. (2019). Marginal climate and air quality costs of aviation emissions. Environmental Research Letters, *14*(11), 114031. https://doi.org/10.1088/1748-9326/ab4942